CHEMISTRY & SUSTAINABILITY
CHEMSUSCHEM
ENERGY & MATERIALS

Supporting Information

Methanol–Water Aqueous-Phase Reforming with the Assistance of Dehydrogenases at Near-Room Temperature

Yangbin Shen,[a] Yulu Zhan,[a] Shuping Li,[a] Fandi Ning,[a] Ying Du,[a] Yunjie Huang,[b] Ting He,[a] and Xiaochun Zhou*[a, c, d]

cssc_201702359_sm_miscellaneous_information.pdf

Author Contributions

X.Z. designed and directed the project. Y.S. carried out catalytic experiments and synthesis of the catalysts, and Y.Z. analyzed the data and performed NMR spectroscopy analysis and TEM and SEM recordings. S.L. performed the UV/Vis detection and analyzed the pore-size distributions and average pore diameters of the catalyst. F.N. performed GC and XPS experiments and analyzed the data. Y.D. collected the XRD data. Y.H. and T.H. analyzed the iridium contents of the catalysts. X.Z. and Y.S. wrote and revised the manuscript.

Table of contents

SI-1. Chemicals and Materials. 3

SI-2. Characterization and physical measurements 4

SI-3. Preparation of Catalysts 5

SI-4. Typical liquid compound for hydrogen generation 6

SI-5. UV-Vis measurement for ADH, ALDH and FDH 7

SI-6. Experiment for hydrogen generation. 8

SI-7. Effect of formaldehyde on the activity of ADH for methanol dehydrogenation. 9

SI-8. Effect of formaldehyde on the activity of FDH for CO_2 hydrogenation. 10

SI-9. Effect of Cp*$IrCl_2$(ppy) on the activity of enzyme. 11

SI-10. TEM image of polypyrrole, Cp^*IrCl_2(ppy) and polypyrrole absorbed Ir nanoparticles 12

SI-11. Effect of polypyrrole Synthesis Temperature (T_{ppy}) on the Catalytic Activity 13

SI-12. Thermal analysis of polypyrrole and Cp^*IrCl_2(ppy) 15

SI-13. ^{1}H-NMR spectrums of Cp*$IrCl_2$(ppy) 16

SI-14. FA dehydrogenation activity measurement 17

SI-15. TOF Calculation. 17

SI-16. Influence of CH_3OH concentration on CH_3OH dehydrogenation catalyzed by ADH 18

SI-17. Influence of 400mM methanol on formaldehyde dehydrogenation catalyzed by ALDH 19

SI-18. Influence of 400 mM methanol on CO_2 hydrogenation catalyzed by FDH 20

SI-19. Influence of 400mM methanol on formic acid dehydrogenation catalyzed by Cp^*IrCl_2(ppy) 21

SI-20. Repeated experiment for hydrogen generation from methanol 22

SI-21. Catalytic activity of Cp*$IrCl_2$(ppy) for 10 mM HCHO decomposition 23

SI-22. References 23

SI-1. Chemicals and Materials.

All chemicals were commercial and used without further purification unless specified. Ethanol (C_2H_5OH, Tianjing Baishi Chemical Industry Co., Ltd, >99.7%), sodium hydroxide (NaOH, Sinopharm Chemical Reagent, Co., Ltd, >96%), 1,2,3,4,5-pentamethylcyclopentadiene ($C_{10}H_{16}$, Sun Chemical Technology(Shanghai) Co., Ltd, 97%), formic acid (HCOOH, Sinopharm Chemical Reagent. Co., Ltd. >98%), pyrrole (C_4H_5N, Shanghai Macklin Biochemical Co., Ltd., >99%), methanol (CH_3OH, Sinopharm Chemical Reagent, Co., Ltd, >99.7%), chloroiridic acid (H_2IrCl_6 $6H_2O$, Shanghai Tuosi Chemical Co., Ltd, Ir wt%>35%), iron(III) chloride ($FeCl_3$, Shanghai Macklin Biochemical Co., Ltd. >99.9%), potassium carbonate (K_2CO_3, Sun Chemical Technology(Shanghai) Co., Ltd, 99%), β-Nicotinamide adenine dinucleotide hydrate(NAD^+, Sigma-Aldrich Co. LLC.,≥98%), β-Nicotinamide adenine dinucleotide, reduced disodium salt hydrate(NADH, J&K Scientific Ltd,98%), N,N-dimethylformamide (DMF, C_3H_7NO, Sinopharm Chemical Reagent, Co., Ltd, >99.5%), diethyl ether ($C_4H_{10}O$, Sinopharm Chemical Reagent, Co., Ltd, >99.5%), ultrapure water was prepared by Thermo PureLab Ultra Genetic.

Enzymes: alcohol dehydrogenase from Saccharomyces cerevisiae (ADH 369 units/mg solid, 383 units/mg protein, molecular weight of ADH (M_{ADH}) =141 kDa, Sigma-Aldrich Co. LLC.), aldehyde dehydrogenase, potassium-activated from baker's yeast (s. cerevisiae) (ALDH 1.8 units/mg solid, 22 units/mg protein, molecular weight of ALDH (M_{ALDH}) =170 kDa, contains lactose, potassium phosphate and citrate buffer salts, and mercaptosuccinic acid, Sigma-Aldrich Co. LLC.). Formate dehydrogenase from Candida boidinii (FDH, liquid, clear brown, Nanjing Sunlidabio Co., Ltd, ~100 U/mL).

One unit (U) is defined as the amount of the enzyme that catalyzes the conversion of 1 micro mole (μmole) of substrate per minute. For example, one unit of ADH could convert 1.0 μmole of ethanol to acetaldehyde per min at pH 8.8 at 25 ℃; one unit of ALDH could oxidize 1.0 μmole of acetaldehyde to acetic acid per min at 25 ℃ and pH 8.0 in the presence of NAD^+.

SI-2. Characterization and physical measurements

^{1}H NMR spectra of catalysts were recorded on Varian Plus 400 MHz. Gas chromatography experiments were performed on GC-G5 chromatograph with FID/TCD and methanizer (Beijing Persee General Instrument Co., Ltd). The system uses N_2 as a carrier gas, allows for the detection limits of the following gases: $H_2 \geq 100$ ppm, CO $\geq$ 1 ppm. The transmission electron microscopy (TEM) images were recorded on Tecnai, 200 kV, G2 F20 S-TWIN, FEI, and the scanning electron microscope images (SEM) were recorded on Quanta 400 FEG, FEI. Thermogravimetric analysis measurement was conducted by TG 209F1 (NETZSCH, Germany), air as carrier gas, gas flow rate is 20 mL min^{-1}, heating rate is 10 K min^{-1}. X-ray photoelectron spectroscopic (XPS) measurements were carried out using a Kratos XSAM-800 spectrometer with a Mg Ka radiator. Powder X-ray diffraction (XRD) patterns of samples were collected by Bruker D8 X-ray diffractometer with the Cu-Kα (λ =1.5406 Å) radiation source operating at 40 kV and 40 mA. The iridium contents of the catalysts were analyzed by element analyzer (vario ELcube, Elementar Analysensysteme GmbH, Germany). UV-absorption and enzymatic reaction kinetics were record by Shimadzu UV-1800. The surface areas of the polypyrrole and Cp^*IrCl_2(ppy) were determined by the Brunauer-Emmett-Teller (BET) method, based on the amount of N_2 adsorbed at pressures $0.05 < P/P_0 < 0.3$. The pore size distributions and average pore diameter of the catalyst were analyzed by the BJH nitro-gen adsorption and desorption method (ASAP 2020, Micromeritics, USA).

SI-3. Preparation of Catalysts

Synthesis of Polypyrrole. The polypyrrole was prepared by chemical polymerization in $FeCl_3$ methanol solution at 10 ℃.[1] The molar ratio of $FeCl_3$ to pyrrole was 2.33:1. The polypyrrole was washed by ultrapure water and dried at room temperature for further use.

Synthesis of $[Cp^*IrCl_2]_2$. Excess 1,2,3,4,5-pentamethylcyclopentadiene was added in H_2IrCl_6 methanol solution. The molar ratio of 1,2,3,4,5-pentamethylcyclopentadiene to H_2IrCl_6 was about 2.5:1. The mixture was stirred under reflux for 37 h, then cooled to 0 ℃. The yellow brown product will be gained after filtration and washed with ether.[2]

Synthesis of Cp^*IrCl_2(ppy). The polypyrrole suspension in excess K_2CO_3 was stirred for 2 h at 55 ℃. Then $[Cp^*IrCl_2]_2$ was added into the suspension, and was kept stirring overnight. The molar ratio of polypyrrole (based on pyrrole monomer) to $[Cp^*IrCl_2]_2$ was 80. The product Cp^*IrCl_2(ppy) was gained after filtration, washed by ultrapure water and dried at room temperature. The Cp^*IrCl_2(ppy) was the novel polymer complex catalyst for HCOOH dehydrogenation. The total process for synthesizing the Cp^*IrCl_2(ppy) was illustrated in **Scheme 2.**

SI-4. Typical liquid compound for hydrogen generation

Table S1. Typical liquid compound for hydrogen generation.

H_2 carrier	H_2 content	$T_{reaction}$	Reaction condition	Conversion rate	CO content	Ref
CH_3OH	12.6 wt%	25℃	Photocatalysis	/	no	3
		25℃	Need O_2	/	no	4
		25℃	Electrocatalysis	/	high	5
		Reflux	Need alkali	84%	/	6
		150 -190 ℃	†	/	≥100ppm	7
HCHO	6.7 wt%	70-95℃	†	> 99%	/	8
HCOOH	4.4 wt%	90℃	HCOONa	>90%	No	9, 10
C_2H_5OH	13.1 wt%	250–600℃	†	100%	high	11
H_2O	11.1wt%	25℃	Electrocatalysis	100%	No	12

† means no extra additives or energy, / means no mentions in the literature

SI-5. UV-Vis measurement for ADH, ALDH and FDH

Representative experiment of methanol dehydrogenation by ADH: 400 μM NAD^+, 400 mM methanol and 500 μL phosphate buffer (pH=8.4) was placed in the cuvette at 25℃, then 30 U ADH was added in the cuvette. The corresponding UV-Vis spectrum and enzyme kinetics was recorded by Shimadzu UV-1800. The generated NADH has characteristic absorption peak at 340 nm.

Representative experiment of formaldehyde dehydrogenation by ALDH: 159 μM NAD^+, 506 μM HCHO and 500 μL phosphate buffer (pH=8.4) was placed in the cuvette at 25℃, then 0.63 U ADLH was added in the cuvette. The generated NADH have characteristic absorption peak at 340 nm.

Representative experiment of $KHCO_3$ hydrogenation by FDH and NADH: 130 μM NADH, 3 mM $KHCO_3$ and 500 μL phosphate buffer (pH=7.3) was placed in the cuvette at 25℃, then 8 U FDH was added in the cuvette. The generated NADH would cause the UV-Vis absorption change at 340 nm during the reaction. The corresponding UV-Vis spectrum and enzyme kinetic parameter was recorded by Shimadzu UV-1800 during the reaction.

Representative experiment of formic acid dehydrogenation by FDH: 160 μM NAD^+, 519.8 μM HCOOH and 500 μL phosphate buffer (pH=7.3) was placed in the cuvette at 25℃, then10 U FDH was added. The generated NADH would cause the UV-Vis absorption change at 340 nm during the reaction.

SI-6. Experiment for hydrogen generation.

Representative experiment: 50 U FDH, 1 U ALDH, 30 U ADH and 4 mg Ir-catalyst were added in a 25 mL flask which had contained 5 mL phosphate buffer (pH=7.5), 4 mM NAD^+. The flask was connected to a u-tube containing $CuSO_4$ solution. Then the nitrogen was blow into the total device for more than 10 minutes, replaced the air inside. At last, the methanol and $KHCO_3$ were injected into the solution after the flask was heated to preset temperature. The gas content was analyzed by the GC every hour. The detail diagram could refer to our previous work.[13]

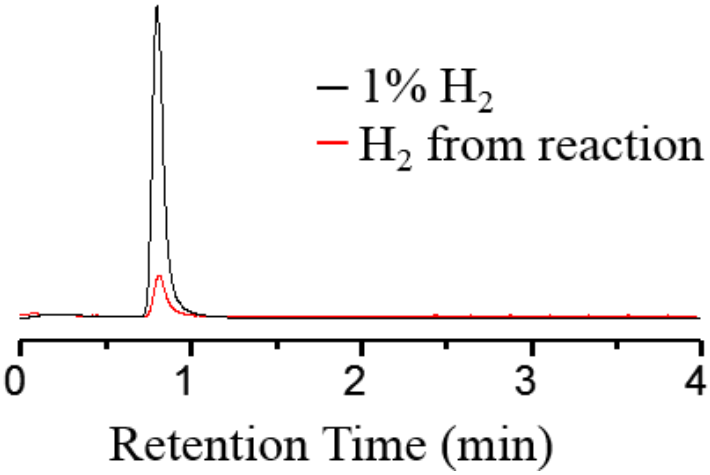

Figure S1. Hydrogen measurement by gas chromatography (GC). Red line: hydrogen from methanol dehydrogenation. Black line: 1 % hydrogen standard sample.

SI-7. Effect of formaldehyde on the activity of ADH for methanol dehydrogenation.

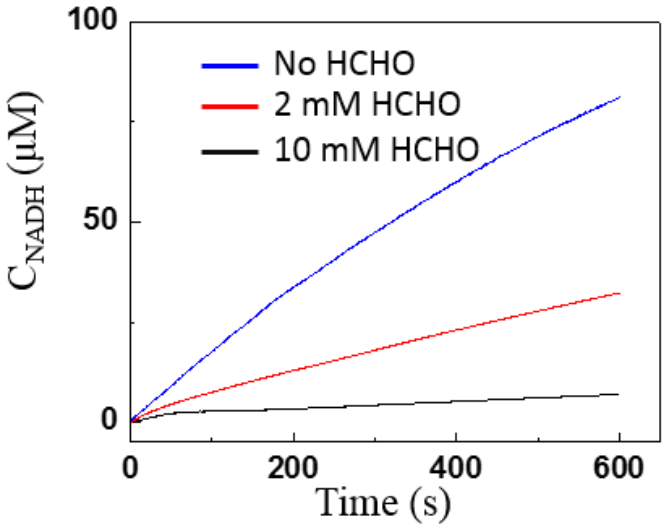

Figure S2 Effect of formaldehyde on the activity of ADH for methanol dehydrogenation. 400 μM NAD^+, 30 U ADH, 300 mM methanol and 500 μL phosphate buffer (pH=8.4) was placed in the cuvette at 25°C.

Figure S2 shows the NADH concentration versus time trajectory during CH_3OH dehydrogenation with different concentrations of formaldehyde. We find too much HCHO could inhibit the activity of ADH for methanol dehydrogenation.

SI-8. Effect of formaldehyde on the activity of FDH for CO_2 hydrogenation.

Figure S3 shows the effect of formaldehyde on CO_2 hydrogenation catalyzed by FDH. We find high concentration HCHO could inhibit the activity of FDH for CO_2 hydrogenation.

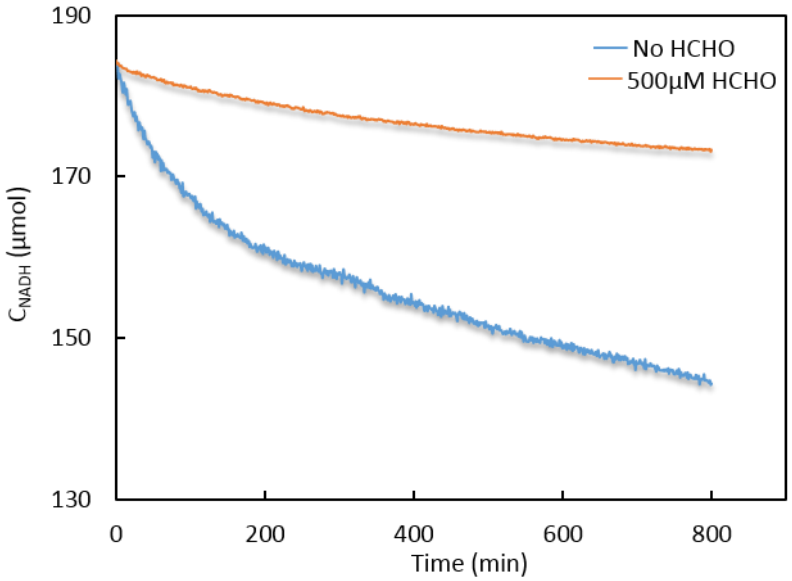

Figure S3. Effect of formaldehyde on the activity of FDH for CO_2 hydrogenation. Condition: 185 μM NADH, 8 U FDH, 3 mM $KHCO_3$, 500 μL phosphate buffer (pH=6.8) was placed in the cuvette at 25℃.

SI-9. Effect of $Cp^*IrCl_2(ppy)$ on the activity of enzyme.

The $Cp^*IrCl_2(ppy)$ will not interact with the active site of enzymes, and show high compatibility to enzymes. As exhibited in **Figure S4**, although the catalyst is mixed with ADH, ALDH and FDH for 12 hours before measuring the activities respectively. But it doesn't have any poisoning effect on its catalytic activity, the enzymes still keep their original catalytic activities for respective reactions.

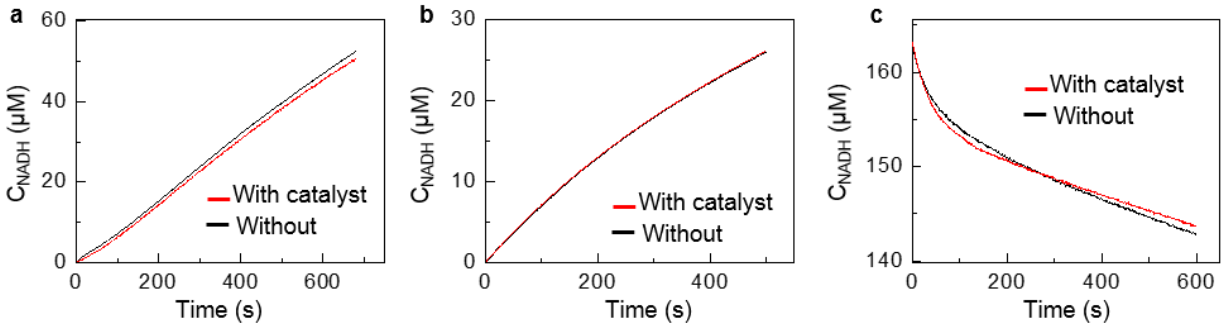

Figure S4. (a) Activity of ADH for methanol dehydrogenation with and without Ir-catalyst $Cp^*IrCl_2(ppy)$. (b) Activity of ALDH for formaldehyde dehydrogenation with and without Ir-catalyst $Cp^*IrCl_2(ppy)$. (c) Activity of FDH for CO_2 hydrogenation with and without Ir-catalyst $Cp^*IrCl_2(ppy)$. The red and black curves are for the measurements with and without Ir-catalyst $Cp^*IrCl_2(ppy)$, respectively.

SI-10. TEM image of polypyrrole, $Cp^*IrCl_2(ppy)$ and polypyrrole absorbed Ir nanoparticles

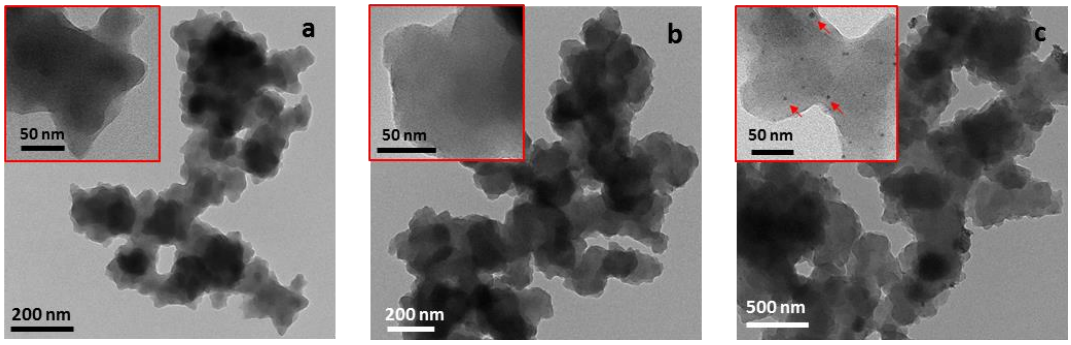

Figure S5. (a) TEM image of polypyrrole. (b) TEM image of $Cp^*IrCl_2(ppy)$. (c) TEM image of polypyrrole absorbed Ir nanoparticles, the arrows in inset point out the nanoparticles.

SI-11. Effect of polypyrrole Synthesis Temperature (T_{ppy}) on the Catalytic Activity

The polypyrrole is one of the main precursors for the synthesis of Cp^*IrCl_2(ppy) catalyst. The property of polypyrrole have a great influence on the catalytic activity. The physical and chemical properties of polypyrrole strongly depend on the synthesis temperature and solvents. Different synthesis conditions may lead to different properties of polypyrrole, such as surface area, electric conductivity, gas sensitivity and pore diameter. In this paper, we mainly studied the effect of synthesis temperature of polypyrrole (T_{ppy}) on the catalytic activity for FA dehydrogenation.

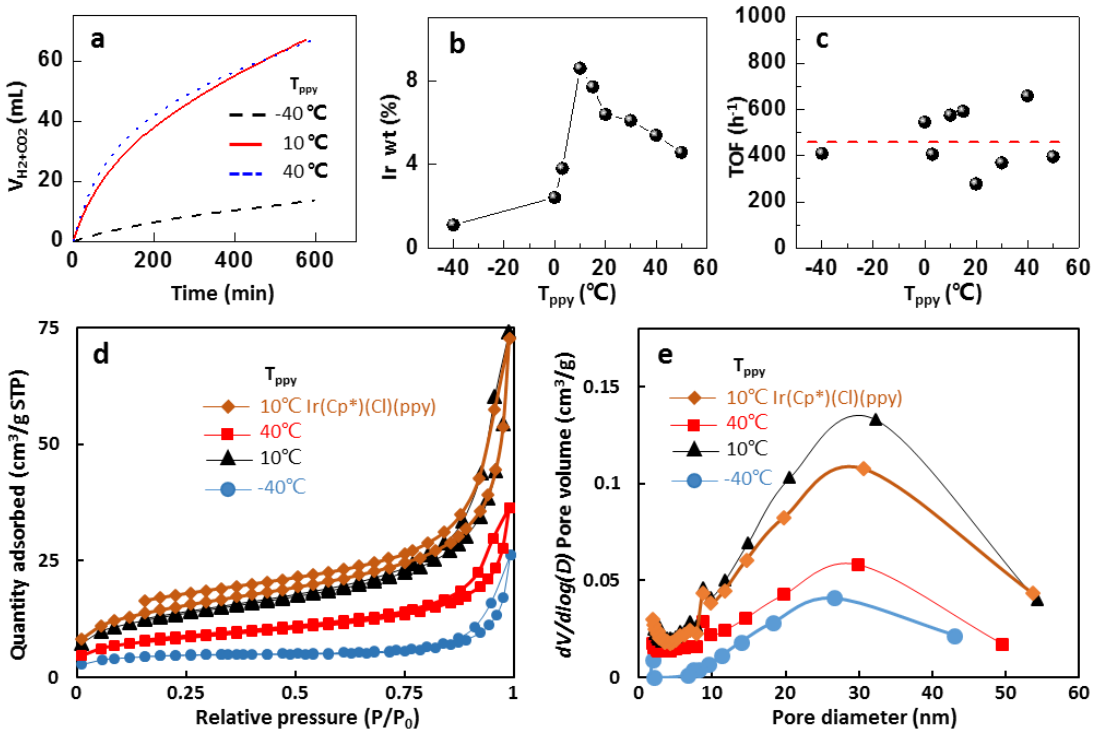

Figure S6. Influence of polypyrrole synthesis temperature (T_{ppy}) on the catalytic activity for FA dehydrogenation. (a) Volume of the evolved gas (V_{CO2+H2}) versus time for three different catalysts, whose polypyrrole precursors were synthesized at different temperature including -40 ℃, 10 ℃ and 40 ℃. (b) Ir content in different catalysts with different T_{ppy}. (c) TOF for the catalysts in **b**. (d) N_2 BET adsorption/desorption isotherms for the polypyrrole precursors synthesized at -40 ℃, 10 ℃ and 40 ℃, and the Cp^*IrCl_2(ppy) catalyst, whose polypyrrole precursor was synthesized at 10 ℃. (e) BJH pore size distribution of the same samples in **d**. The FA dehydrogenation was catalyzed by

$Cp^*IrCl_2(ppy)$ (2.3 mg) with 1.0 M FA (without SF) at 35 ℃.

In this section, the synthesis condition of $Cp^*IrCl_2(ppy)$ catalysts was the same for different polypyrrole precursors, and the molar ratio of polypyrrole (based on pyrrole monomer) to $[Ir(Cp^*)(Cl)_2]_2$ is 50. The polypyrrole precursors were synthesized at different temperature from -40 to 50 ℃. **Figure S6a** shows the gas volume (CO_2+H_2) versus time evolved by 3 different $Cp^*IrCl_2(ppy)$ catalysts at 35 ℃. The polypyrrole precursors used in these three catalysts were synthesized at different temperature including -40, 10 and 40 ℃. The catalysts synthesized by 10 and 40 ℃ ppy precursors have higher activity.

In order to find the reason for the notable difference, Ir content in these $Cp^*IrCl_2(ppy)$ catalysts was measured by element analyzer (vario ELcube, Elementar Analysensysteme GmbH, Germany). **Figure S6b** exhibits that the Ir content in these catalysts varies significantly, and has a peak value for the polypyrrole synthesized at 10 ℃. The variation of Ir content indicates that the polypyrrole synthesized at different temperature has different ability to coordinate with $[Ir(Cp^*)(Cl)_2]_2$. However, **Figure S6c** shows that the TOF values for these catalysts are all around 450 h^{-1}, which are independent on the apparent activity and Ir content. Hence, these catalysts may have similar catalytic active site containing $Ir(Cp^*)$ group.

In order to investigate the notable difference of Ir content, the polypyrrole and catalyst were characterized by N_2 BET adsorption/desorption isotherms. **Figure S6d** shows that the specific surface areas of polypyrrole synthesized at -40, 10 and 40 ℃ are 14.9 m^2 g^{-1}, 45.5 m^2 g^{-1} and 27.9 m^2 g^{-1}, respectively. The polypyrrole synthesized at 10 ℃ has much larger specific surface area comparing to the others. Because the $Cp^*IrCl_2(ppy)$ catalyst is synthesized through the solid polypyrrole and dissolved $[Ir(Cp^*)(Cl)_2]_2$, only the sites on the surface of polypyrrole have the ability to react with $[Ir(Cp^*)(Cl)_2]_2$ to form catalytic active site. The polypyrrole synthesized at 10 ℃ would provide more sites reacting with $[Ir(Cp^*)(Cl)_2]_2$ due to its high specific surface area. As a result, the polypyrrole synthesized at 10 ℃ has the highest Ir content in **Figure S6b.** The specific surface area of $Cp^*IrCl_2(ppy)$ catalyst (51.0 m^2 g^{-1}) doesn't change much comparing to its polypyrrole precursor.

Figure S6e shows that the average pore size of polypyrrole synthesized at -40, 10 and 40 ℃ are 22.5 nm, 12.8 nm and 10.6 nm, respectively. The average pore diameter of polypyrrole decreases

when the T_{ppy} increased. The average pore diameter of Cp^*IrCl_2(ppy) catalyst decreases to 11.4 nm comparing to its polypyrrole precursor synthesized at T_{ppy}=10 ℃. The decrease of pore diameter may be due to the binding of $[Ir(Cp^*)(Cl)_2]_2$ on the wall of pore in polypyrrole. This also indicates that the pore in polypyrrole has high ability to react with $[Ir(Cp^*)(Cl)_2]_2$ inducing large number of active sites in the pore.

SI-12. Thermal analysis of polypyrrole and Cp^*IrCl_2(ppy)

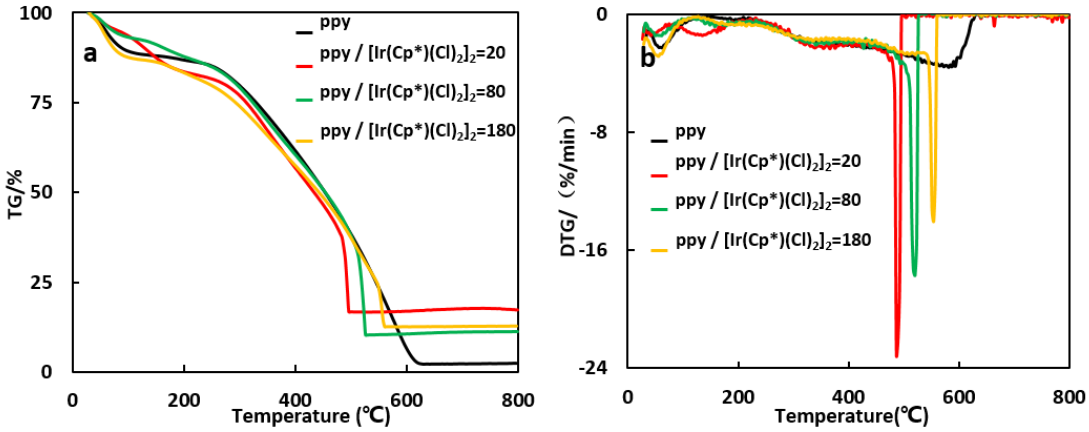

Figure S7. (a) TG pattern of polypyrrole and different Cp^*IrCl_2(ppy). (b) DTG pattern of polypyrrole and different Cp^*IrCl_2(ppy). The molar ratios of polypyrrole (based on pyrrole monemer) to $[Ir(Cp^*)(Cl)_2]_2$ are 20, 80 and 180, respectively. The Ir contents in these three catalysts Ir wt% are 9.87%, 4.26% and 2.31%.

Figure S7 gives the thermal analysis data of these different Cp^*IrCl_2(ppy) and polypyrrole. **Figure S7a** shows the TG patterns of three Cp^*IrCl_2(ppy) catalysts with different Ir contents have the similar TG curve. They all have a sharp weight losing process comparing to polypyrrole. The catalysts would decompose rapidly at a special temperature and then tend to keep stable. Interestingly, the more Ir the catalyst contains, the lower special temperature will appear. We infer the site of polypyrrole and $Ir(Cp^*)$ would thermolyze rapidly, resulting in the above phenomenon. **Figure S7b** gives the DTG data of polypyrrole and Cp^*IrCl_2(ppy). Three Cp^*IrCl_2(ppy) catalysts with different Ir contents have the similar DTG curve.

SI-13. ^{1}H-NMR spectrums of Cp*IrCl$_2$(ppy)

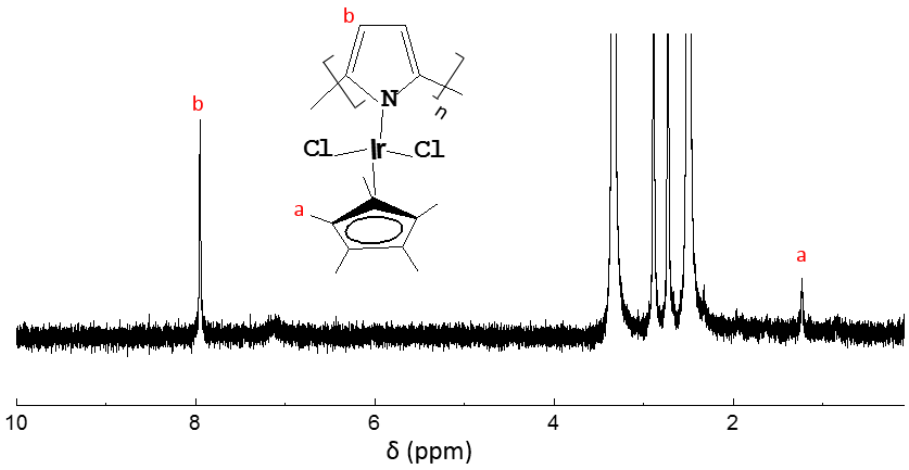

Figure S8. ^{1}H-NMR spectrums of the Cp*IrCl$_2$(ppy). ^{1}H NMR ((CD$_3$)$_2$SO, 400 MHz) δ_H: 1.23 (s), 7.94 (d).

^{1}H NMR spectra of catalysts was recorded on Varian Plus 400 MHz. The Cp*IrCl$_2$(ppy) is a kind of insoluble polymer. Although we employed (CD$_3$)$_2$SO to dissolve this polymer, but it still couldn't be well dissolve. We only could collect the weak ^{1}H NMR signal, and the **a** and **b** signal in **Figure S8** could attribute to –CH$_3$ and pyrrole. Additionally, the NMR signal of Cp*IrCl$_2$(ppy) can't collect on a solid-state high-resolution NMR spectroscopy, because the catalyst is conductive material.

SI-14. FA dehydrogenation activity measurement

The FA dehydrogenation was performed in a one-necked round-bottomed flask. The flask is heated in a water bath at a preset temperature (25-80℃) under ambient atmosphere. The catalyst powder would be injected into the flask though a Teflon tube by syringe. The tube is immerged in the FA solution in case of air leakage. The gas generation rate could be measured by a graduated buret or a 100 mL syringe, and was recorded by a digital camera.

SI-15. TOF Calculation.

The TOF calculation here was based on the number of Ir atoms in catalyst. The calculation of $V_{m,H2,20℃}$ was carried out using van der Waals of hydrogen by **Equation 1**.

$$V_{m,H2,20℃} = \frac{RT}{p} + b - \frac{a}{RT} = 24.2 \text{ L/mol} \approx 24 \text{ L/mol} \quad (1)$$

R is 8.3145 m ^{3}Pa mol^{-1} K^{-1}, T is 293.15 K, p is 101325 Pa, b is 26.7 x 10^{-6} m^3 mol^{-1}, a is 2.49 x 10^{-10} Pa m^3 mol^{-2}.

The calculation of $V_{m,CO2,20℃}$ was carried out using van der Waals of hydrogen by **Equation 2**.

$$V_{m,CO2,20℃} = \frac{RT}{p} + b - \frac{a}{RT} = 24.1 \text{ L/mol} \approx 24 \text{ L/mol} \quad (2)$$

R is 8.3145 m ^{3}Pa mol^{-1} K^{-1}, T is 293.15 K, p is 101325 Pa, b is 42.7 x 10^{-6} m^3 mol^{-1}, a is 36.5 x 10^{-10} Pa m^3 mol^{-2}.

The calculation equation for TOF calculation is[14]

$$TOF = \frac{V/(2*t*24)}{n_{Ir}} \quad (3)$$

V is the volume of generated gas. t is the reaction time during the formaldehyde decomposition, n_{cat} is the molar number of catalyst.

SI-16. Influence of CH_3OH concentration on CH_3OH dehydrogenation catalyzed by ADH

The CH_3OH would be catalytic dehydrogenation by ADH, produce HCHO and NADH. During the reaction, the NAD^+ would be reduced to NADH, which would lead to absorbance change at 340 nm on UV-Vis spectrophotometer.

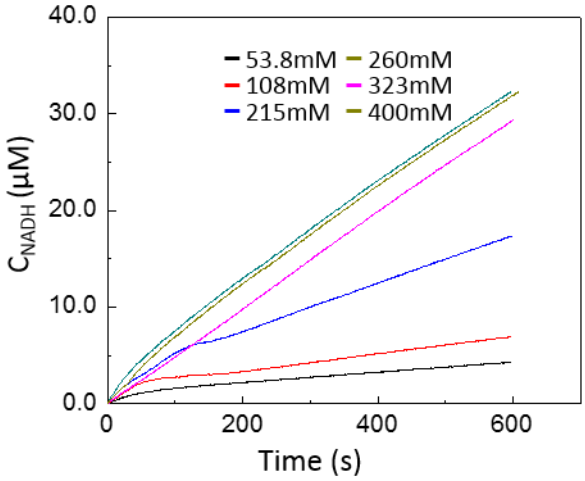

Figure S9. NADH concentration versus time during CH_3OH dehydrogenation catalyzed by ADH under different CH_3OH concentration. Conditions: 346 μM NAD^+, reaction carried out in 500 μL phosphate buffer (pH=9.0) contain 16 U ADH at 25℃.

Figure S9 exhibited the variation of NADH concentration versus time during CH_3OH dehydrogenation. When the CH_3OH concentration is below 260 mM, increasing concentration would accelerate reaction rate. While the concentration is higher than 260 mM, increasing concentration would show no meaning for accelerating reaction rate. So, the Michaelis constant of the ADH for CH_3OH dehydrogenation is 130 mM, which is accordance with the information provided by Sigma-Aldrich Co. LLC.

SI-17. Influence of 400mM methanol on formaldehyde dehydrogenation catalyzed by ALDH

The HCHO could react with water catalyzed by ALDH, generate HCOOH and NADH. During the HCHO dehydrogenation, the NAD^+ would be reduced to NADH, which would lead to absorbance change at 340 nm on UV-Vis spectrophotometer.

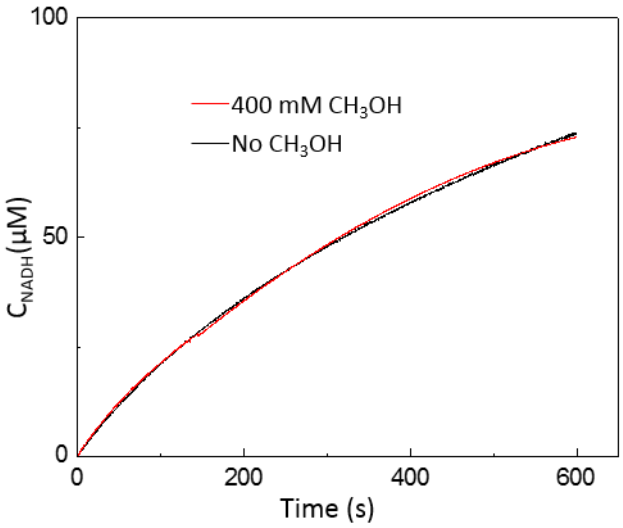

Figure S10. NADH concentration versus time during formaldehyde dehydrogenation catalyzed by ALDH under different condition. Black line conditions: [NAD^+] = 1 mM, [HCHO] = 1 mM ,0.63 U ADLH. Red line conditions: [NAD^+] = 1 mM, [CH_3OH] = 400 mM, [HCHO] = 1 mM, 0.63 U ADLH. Both reaction carried out in 500 μL phosphate buffer (pH=8.0) at 25 ℃.

In order to analyze the influence of 400 mM methanol on formaldehyde dehydrogenation catalyzed by ALDH. We carried out the contrastive experiments. We find the low concentration methanol have little effect on the formaldehyde dehydrogenation. Therefore, there is no need to take the low concentration methanol into consideration during the formaldehyde dehydrogenation.

SI-18. Influence of 400 mM methanol on CO_2 hydrogenation catalyzed by FDH

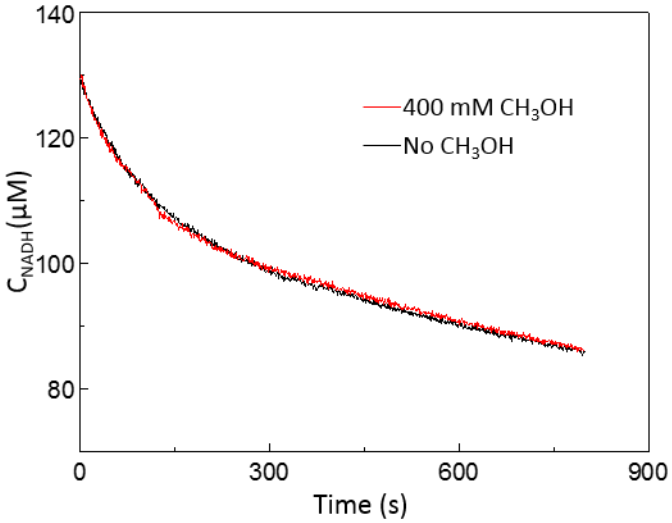

Figure S11. NADH concentration versus time during CO_2 hydrogenation catalyzed by FDH under different condition. Black line conditions: [NADH] = 130 μM, [$KHCO_3$] = 3 mM. Red line condition: [NADH] = 130 μM, [$KHCO_3$] = 3 mM, [CH_3OH] = 400 mM. Both experiments reaction carried out in 500 μL phosphate buffer (pH=6.8) contain 8 U FDH at 25℃.

For studying the influence of 400 mM methanol on the CO_2 hydrogenation catalyzed by FDH, we carried out the contrastive experiments. During the reduction reaction, the NADH would be oxidized to NAD^+, which leaded to absorbance decrease at 340 nm on UV-Vis spectrophotometer, as 340 nm was the characteristic absorption peak of NADH. We find the low concentration methanol didn't inhibit the activity of FDH for CO_2 hydrogenation. Therefore, we could neglect methanol interference on the CO_2 hydrogenation catalyzed by FDH.

SI-19. Influence of 400mM methanol on formic acid dehydrogenation catalyzed by $Cp^*IrCl_2(ppy)$

For studying the influence of 400 mM methanol on the formic acid dehydrogenation, we carried out the contrastive experiments. We find the low concentration methanol have little effect on the reaction rate of formic acid decomposition. Therefore, we could neglect methanol interference on the catalytic activity of $Cp^*IrCl_2(ppy)$.

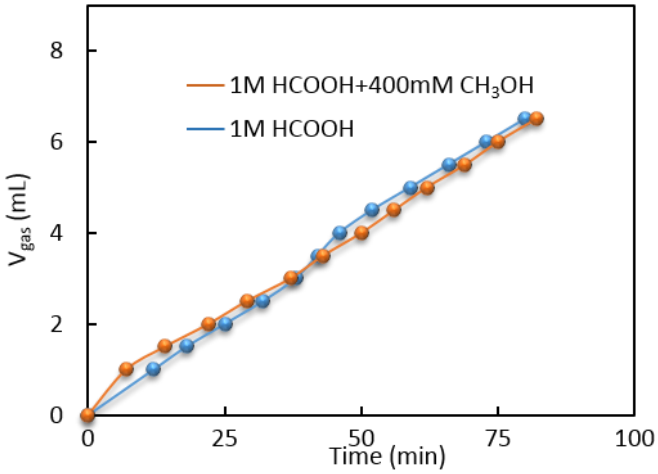

Figure S12. Gas generation process from formic acid dehydrogenation under different condition. Blue line condition: 1 M HCOOH, 5 mL reaction solution. Brown line condition: 1 M HCOOH, 400 mM CH_3OH, 5 mL reaction solution, temperature 25 ℃, Ir-catalyst 3 mg.

SI-20. Repeated experiment for hydrogen generation from methanol

The influence factors of the experiments include enzyme species (ADH, ALDH and FDH), temperature, and pH. Therefore, the reproducibility of the experiments depends on the temperature and pH value if the same enzyme species was employed. The deviation was very small (**Figure S13**), indicating the reproducibility of the experiments is well when the keep the same reaction condition.

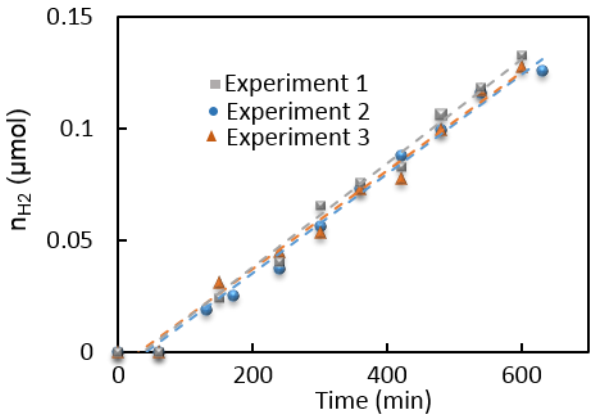

Figure S13. Repeated experiment for hydrogen generation from methanol. The reaction was carried out in 5 mL phosphate buffer containing 400 mM CH_3OH, 20 mM $KHCO_3$, 4 mM NAD^+, 4.0 mg Ir-catalyst, 50 U FDH, 1 U ALDH and 30 U ADH. The reaction was protected by N_2 atmosphere. The pH was kept at 7.50, and temperature is 29℃.

SI-21. Catalytic activity of Cp*IrCl$_2$(ppy) for 10 mM HCHO decomposition

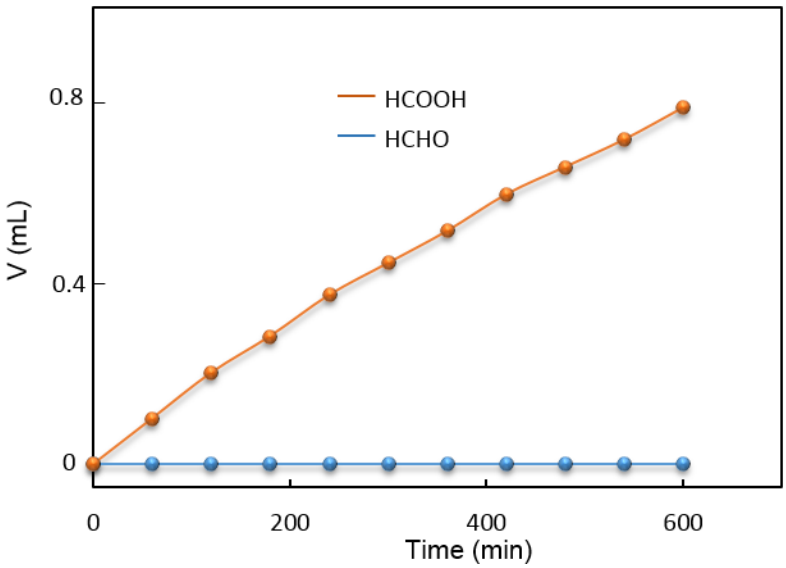

Figure S14. Evolved gas volume variation during the reaction. Blue condition: 10 mM HCHO, 5 mL reaction solution, 5mg Cp*IrCl$_2$(ppy), pH=7. Brown condition: 10 mM HCOOH, 5 mL reaction solution, 5 mg Cp*IrCl$_2$(ppy). Reaction temperature is 30 ℃.

No volume variation was occurred during the formaldehyde dehydrogenation catalyzed by Cp*IrCl$_2$(ppy), we also analyzed the gas components by GC in the reactor, no hydrogen was detected, indicating the Cp*IrCl$_2$(ppy) have little catalytic for the hydrogen generation from 10 mM formaldehyde. While the Ir-catalyst showed good catalytic activity for the formic acid dehydrogenation.

SI-22. References

[1] S. Machida, S. Miyata, A. Techagumpuch *Synthetic Metals*. **1989**, *31*, 311-318.
[2] S. Fukuzumi, T. Kobayashi, T. Suenobu *Journal of the American Chemical Society*. **2010**, *132*, 1496-1497.
[3] Z. Liu, Z. Yin, C. Cox, M. Bosman, X. Qian, N. Li, H. Zhao, Y. Du, J. Li, D. G. Nocera *Science Advances*. **2016**, *2*.
[4] L. E. Heim, D. Thiel, C. Gedig, J. Deska, M. H. G. Prechtl *Angewandte Chemie-International Edition*. **2015**, *54*, 10308-10312.
[5] J. Gonzalez-Cobos, V. J. Rico, A. R. Gonzalez-Elipe, J. L. Valverde, A. de Lucas-Consuegra *ACS Catalysis*. **2016**, *6*, 1942-1951.

[6] K.-i. Fujita, R. Kawahara, T. Aikawa, R. Yamaguchi *Angewandte Chemie-International Edition*. **2015**, *54*, 9057-9060.
[7] L. Lin, W. Zhou, R. Gao, S. Yao, X. Zhang, W. Xu, S. Zheng, Z. Jiang, Q. Yu, Y.-W. Li, C. Shi, X.-D. Wen, D. Ma *Nature*. **2017**, *544*, 80-+.
[8] L. E. Heim, S. Vallazza, D. van der Waals, M. H. G. Prechtl *Green Chemistry*. **2016**, *18*, 1469-1474.
[9] W. Wang, T. He, X. Liu, W. He, H. Cong, Y. Shen, L. Yan, X. Zhang, J. Zhang, X. Zhou *ACS applied materials & interfaces*. **2016**, *8*, 20839-20848.
[10] Y. Du, Y.-B. Shen, Y.-L. Zhan, F.-D. Ning, L.-M. Yan, X.-C. Zhou *Chinese Chemical Letters*. **2017**, *28*, 1746-1750.
[11] V. Palma, F. Castaldo, P. Ciambelli, G. Iaquaniello *Applied Catalysis B-Environmental*. **2014**, *145*, 73-84.
[12] V. S. Thoi, Y. Sun, J. R. Long, C. J. Chang *Chemical Society Reviews*. **2013**, *42*, 2388-2400.
[13] Y. Zhan, Y. Shen, S. Li, B. Yue, X. Zhou *Chemical Communications*. **2017**, *53*, 4230-4233.
[14] Q. L. Zhu, N. Tsumori, Q. Xu *Journal of the American Chemical Society*. **2015**, *137*, 11743-11748.